RESEARCH ARTICLE

Synthesis, structure, and superconductivity of B-site doped perovskite bismuth lead oxide with indium†‡

Xiande Zheng, [iD] [b] Lei Zhang,[a] Xiaoge Wang,[a] Yiguo Qing,[c] Jie Chen,[d] Yaoda Wu,[d] Sihao Deng,[d] Lunhua He,[d,e,f] Fuhui Liao,[a] Yan Wang,[a] Jinling Geng,[a] Junliang Sun, [iD] [a] Guobao Li, [iD] *[a] Laijun Liu [iD] *[b] and Jianhua Lin*[a]

Many elements can be doped into the A site of perovskite $BaBiO_3$-based superconductors, but only Bi, Pb, Tl, Sb, Mg, and Na are found in the B site. Here, the successful synthesis of $Ba(Bi_{0.25}Pb_{0.75})_{1-x}In_xO_{3-\delta}$ superconductors by solid state reaction provides an example with indium located in the B site. The X-ray, neutron, and selected area electron diffraction data indicate that all the samples crystallize in the non-centrosymmetric space group $P1$ at room temperature. The superconductive transition temperature T_c^{zero} of $Ba(Bi_{0.25}Pb_{0.75})_{1-x}In_xO_{3-\delta}$ decreases with an increase of indium, which is attributed to the fact that the hole concentration in the samples departs from the optimal hole doping state of $BaBi_{0.25}Pb_{0.75}O_{3-\delta}$ superconductor.

Introduction

Since the discovery of superconductivity in perovskite $BaBi_{1-y}Pb_yO_{3-\delta}$,[1] studies on perovskite superconductors have continued to date because they are the only high-temperature oxide superconductors to show fully three-dimensional conductivity and are very different from the well-studied cuprate superconductors and iron-based superconductors showing two-dimensional conductivity. The typical ones include $Ba_{1-x}K_xBiO_3$ $(0.30 < x < 0.45)$,[2,3] $(Na_{0.25}K_{0.45})Ba_3Bi_4O_{12}$,[4] $Ba_{1-x}K_zBi_{1-y}Pb_yO_3$,[5,6] $Ba_{0.9}K_xBiO_3$,[7] $Ba_{1-x}Ln_x(Bi_{0.20}Pb_{0.80})O_{3-\delta}$ (Ln = Y, La, Ce, Pr, Nd, Sm, Eu, Gd, Tb, Dy, Ho, Er, Tm, Yb, Lu),[8,9] $Ba_{0.85-x}La_xPr_{0.15}(Bi_{0.20}Pb_{0.80})O_{3-\delta}$,[10]

$KBa_3(Bi_{0.89}Na_{0.11})_4O_{12}$,[11] $BaBi_{0.25}Tl_{0.25}Pb_{0.50}O_{3-\delta}$,[12] $(K_{0.87}Bi_{0.13})BiO_3$,[13] $Sr_{1-x}K_xBiO_3$,[14] $Ba_{0.82}K_{0.18}Bi_{0.53}Pb_{0.47}O_3$,[15] $Ba_{0.62}K_{0.38}Bi_{0.92}Mg_{0.08}O_3$,[16] $BaSb_{0.25}Pb_{0.75}O_3$,[17] $La_{0.2}K_{0.8}BiO_3$,[18] $Sr_{0.5}Rb_{0.5}BiO_3$,[14] and so on. Most of these superconductors are usually denoted as $BaBiO_3$-based superconductors except $BaSb_{0.25}Pb_{0.75}O_3$. Many elements can be doped into the A site of $BaBiO_3$-based perovskite superconductors, but only Sb, Tl, Pb, Bi, Mg, and Na are found in the B site, although many other elements can be doped into the B site to form a $BaBiO_3$-based perovskite nonsuperconductor.[19–21] Is there a rule to select the specific elements to be doped in the B site of $BaBiO_3$-based perovskite superconductors? Let us look for some similarities among the elements in the B site of $BaBiO_3$-based perovskite superconductors. Tl, Pb, and Bi belong to the same row in the periodic table. Therefore, Tl^{3+}, Pb^{4+} and Bi^{5+} have the same electronic structure. This may be the reason why they can coexist in the B site to maintain the superconductivity.[12] Sb is just above Bi in the same column of the periodic table. The electronic structure of Sb^{5+} is very similar to those of Bi^{5+} and Pb^{4+}. Therefore, $BaSb_{0.25}Pb_{0.75}O_3$ is found to be a superconductor[17] similar to $BaBi_{0.25}Pb_{0.75}O_3$. Following these ideas, In^{3+} and Sn^{4+} have a chance to coexist in the B site of a perovskite superconductor because the electronic structures of In^{3+} and Sn^{4+} are the same as that of Sb^{5+}. Herein, by using the hole-doping superconductor $BaBi_{0.25}Pb_{0.75}O_{3-\delta}$ as a starting perovskite compound,[22] we have synthesized hole-overdoped superconductors $Ba(Bi_{0.25}Pb_{0.75})_{1-x}In_xO_{3-\delta}$ with In^{3+} successfully doped into the B site. The present results support the fact that similar electronic structure seems to benefit the keeping

[a]*Beijing National Laboratory for Molecular Sciences, State Key Laboratory of Rare Earth Materials Chemistry and Applications, College of Chemistry and Molecular Engineering, Peking University, Beijing 100871, People's Republic of China. E-mail: Liguobao@pku.edu.cn*

[b]*College of Materials Science and Engineering, Guilin University of Technology, Guilin 541004, People's Republic of China*

[c]*Beijing No. 80 High School, Beijing 100102, People's Republic of China*

[d]*Spallation Neutron Source Science Center, Dongguan, 523803, People's Republic of China*

[e]*Beijing National Laboratory for Condensed Matter Physics, Institute of Physics, Chinese Academy of Sciences, Beijing 100190, People's Republic of China*

[f]*Songshan Lake Materials Laboratory, Dongguan 523808, People's Republic of China*

†In celebration of the 110th anniversary of the College of Chemistry and Molecular Engineering of Peking University
‡Electronic supplementary information (ESI) available: The refinement details of the X-ray diffraction data and the temperature resistivity of the samples. See DOI: 10.1039/d0qi00828a

This journal is © the Partner Organisations 2020

Inorg. Chem. Front., 2020, **7**, 3561–3570 | **3561**

of superconductivity of $BaBiO_3$-based perovskite superconductors with B site doping.

Experimental

Samples with the nominal formula $Ba(Bi_{0.25}Pb_{0.75})_{1-x}In_xO_{3-\delta}$ (x = 0.00, 0.01, 0.02, 0.03, 0.04, 0.05, 0.06, 0.07, 0.08, 0.09, 0.10, 0.12, and 0.14, denoted as In1, In2, ..., and In13, respectively) have been synthesized. The raw materials were In_2O_3 (99.99%), $BaCO_3$ (A.R.), Bi_2O_3 (A.R.), and PbO (A.R.). The oven-dried reagents were homogenized by about thirty minutes of grinding using an agate mortar and a pestle. Usually the weight of each sample is about 10 g. The mixtures were sintered first at 760 °C for 12 hours. Then, the reacted powders were pressed into pellets under 30 MPa and sintered at 780 °C for 12 hours. The sintered mass was again crushed, pulverized, and pressed into cylindrical pellets to undergo three 12 hour heat treatments at 780 °C (In1), 800 °C (In2 and In3), 840 °C (In4, In5, In6, In7, In8, and In9) and 880 °C (In10, In11, In12, and In13), followed by furnace cooling every time with intermediate grinding and then pressing into pellets under 30 MPa. All the treatments were performed in air. Powder X-ray diffraction (PXRD) data were collected on a PANalytical x'Pert[3] Powder with Cu Kα (λ_1 = 0.15405 nm and λ_2 = 0.15443 nm) radiation (2θ range: 5–120° for 2 hours; step: 0.0131°) at 40 kV and 40 mA at room temperature. Neutron diffraction data were collected on the GPPD of the Spallation Neutron Source Science Center at Dongguan, China. The X-ray and neutron diffraction data were analyzed using GSAS software.[23,24] Selected area electron diffractions (SAEDs) were carried out on JEM2100 with an accelerating voltage of 200 kV. The X-ray photoelectron spectroscopy (XPS) patterns were obtained using a UK Kratos Axis Ultra spectrometer with an Al Kα X-ray source operated at 15 kV and 15 mA. The chamber pressure was less than 5.0×10^{-9} Torr. Electron binding energies were calibrated against the C 1s emission at E_b = 284.8 eV. The resistivities of the samples were investigated using a cryogenic Physical Property Measurement System (PPMS, supplied by East Changing, China) from 2 to 50 K. IR spectra were recorded on an FTIR spectrophotometer in the region of 900–150 cm^{-1}. Raman spectra were recorded on a Micro Raman Imaging spectrometer DXRxi in the region of 1200–50 cm^{-1}.

Results and discussion

Structure of $Ba(Bi_{0.25}Pb_{0.75})_{1-x}In_xO_{3-\delta}$

Powder X-ray diffraction patterns of $Ba(Bi_{0.25}Pb_{0.75})_{1-x}In_xO_{3-\delta}$ are similar to that of $BaBi_{0.25}Pb_{0.75}O_{3-\delta}$, as shown in Fig. 1, which indicates that the structure of these samples may be the same as $BaBi_{0.25}Pb_{0.75}O_{3-\delta}$. However, there are diverse reports on the structure of $BaBi_{0.25}Pb_{0.75}O_{3-\delta}$ in the literature. D. E. Cox and A. W. Sleight[25,26] proposed the space group $I4/mcm$ with $a = b \approx 6.047$ Å, and $c \approx 8.063$ Å to describe the structure of $BaBi_{0.25}Pb_{0.75}O_{3-\delta}$ by neutron diffraction, which was fol-
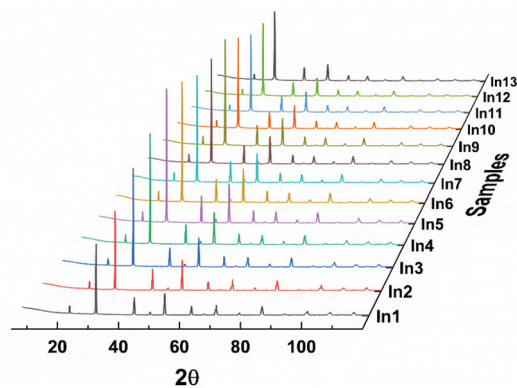

Fig. 1 X-ray diffraction data of $Ba(Bi_{0.25}Pb_{0.75})_{1-x}In_xO_{3-\delta}$. ($x$ = 0.00, 0.01, 0.02, 0.03, 0.04, 0.05, 0.06, 0.07, 0.08, 0.09, 0.10, 0.12, and 0.14 for In1, In2, ..., and In13, respectively).

lowed by that of J. Bredthauer *et al.*[27] Y. Khan *et al.*[28] have suggested a $Cmm2$ space group with $a \approx 6.076$ Å, $b \approx 6.097$ Å and $c \approx 4.291$ Å for $BaBi_{0.25}Pb_{0.75}O_{3-\delta}$. (The X-ray diffraction patterns expected by this model are very different from the obtained X-ray diffraction patterns shown in Fig. 1. Therefore, it is not discussed further.) M. Oda *et al.*[29–31] suggested that the weak difference of oxygen deficiency in the sample could induce the change of tetragonal $BaBi_{0.25}Pb_{0.75}O_{3-\delta}$ with the $I4/mcm$ space group ($a = b \approx 6.047$ Å, and $c \approx 8.063$ Å) to orthorhombic $BaBi_{0.25}Pb_{0.75}O_{3-\delta'}$ with the $Ibmm$ space group ($a \approx 6.072$ Å, $b \approx 6.055$ Å, and $c \approx 8.544$ Å), which had been confirmed by T. Hashimoto *et al.*[32–34] J. Ihringer *et al.*[35] suggested a monoclinic space group $I2/m$ with $a \approx 6.095$ Å, $b \approx 6.095$ Å, $c \approx 8.567$ Å, and $\gamma \approx 90.04°$ for $BaBi_{0.25}Pb_{0.75}O_{3-\delta}$ around room temperature. T. Hashimoto *et al.*[36] suggested that the space group should be Im with $a \approx 6.077$ Å, $b \approx 6.058$ Å, $c \approx 8.554$ Å, and $\gamma \approx 90.00°$. Further, E. Climent-Pascual *et al.*[37] suggested that $BaPb_{1-x}Bi_xO_{3-\delta}$ with $0.2 \leq x \leq 0.3$ was a dimorphic rather than a phase-separated system, showing the coexistence of tetragonal and orthorhombic polymorphs of the same composition but not chemical phase separation. This suggestion may be useful for the samples quenching too quickly to let the high temperature polymorph translate completely into the low temperature polymorph. In this case, two polymorphs with almost the same composition may coexist. However, this kind of sample can be a single phase or a phase-separated system with multiple phases if it is annealed at a suitable temperature for a long time. E. Climent-Pascual's suggestion[37] is not applicable for the samples annealed for a long time, which were used by several researchers including us.

To clarify the structure of $BaBi_{0.25}Pb_{0.75}O_{3-\delta}$, a systemic structural study on $BaBi_{1-y}Pb_yO_{3-\delta}$ ($0.00 \leq y \leq 1.00$)[5,20] has been performed in our lab. As an end member of the series $BaBi_{1-y}Pb_yO_{3-\delta}$, the structure of $BaBiO_{3-\delta}$ has been described as an orthorhombic,[1] rhombohedral,[38] monoclinic,[39] and triclinic[40] distortion of a simple cubic perovskite cell with one Ba, one Bi, and three O in the unit cell by X-ray diffraction data only. Later, $BaBiO_{3-\delta}$ was reported to crystallize in the $I2/$

3562 | *Inorg. Chem. Front.*, 2020, **7**, 3561–3570

This journal is © the Partner Organisations 2020

m space group at room temperature containing both Bi^{3+} and Bi^{5+} with a rock salt-like ordering in a perovskite-type framework using neutron diffraction and/or synchrotron X-ray diffraction.[41–47] The corresponding lattice parameters are similar to $a \approx 6.186$ Å, $b \approx 6.141$ Å, $c \approx 8.672$ Å, and $\beta \approx 90.16°$ at room temperature.[44] Four Ba, four Bi, and twelve O are in the unit cell with one Ba, two Bi, and two O being crystallographically independent. However, S. Sugai[48] suggested that an inversion center is absent in the crystal structure of $BaBiO_{3-\delta}$ from the Raman and infrared reflection spectra of a single crystalline specimen. T. Hashimoto *et al.*[49] further suggested that the space group of $BaBiO_{3-\delta}$ should be $P1$ with the suggested lattice parameters of $a \approx 6.188$ Å, $b \approx 6.139$ Å, $c \approx 8.671$ Å, $\alpha \approx 89.99°$, $\beta \approx 90.14°$, and $\gamma \approx 90.02°$ at room temperature by convergent-beam electron diffraction (CBED) and synchrotron X-ray diffraction. This diversity lead to a confirming study on the symmetry of $BaBiO_{3-\delta}$ by the combined use of selected area electron diffraction (SAED), convergent-beam electron diffraction (CBED), neutron powder diffraction (NPD) with two different wavelengths (λ = 1.6215 and 2.4395 Å), powder X-ray diffraction (PXRD) data with a single wavelength (Cu Kα1, λ = 1.5407 Å), IR spectra, and Raman spectra.[20] The corresponding result shows that $BaBiO_{3-\delta}$ synthesized in our lab crystallizes in the $P1$ space group with $a \approx 6.141$ Å, $b \approx 6.186$ Å, $c \approx 6.144$ Å, $\alpha \approx 59.90°$, $\beta \approx 59.98°$, and $\gamma \approx 59.87°$, which is about half of the T. Hashimoto's $P1$ space group in the volume of unit cell.[49] Two Ba, two Bi, and six O are contained in the unit cell. All of them are crystallographically independent. This unit cell is the smallest one to describe the structure of $BaBiO_{3-\delta}$ with Bi^{3+} and Bi^{5+} at different crystallographically independent sites. Further studies show that this structural model can be also used to describe the structure of $BiFeO_{3-\delta}$ and $BaTbO_{3-\delta}$.[21,50,51] However, this $P1$ space group is not applicable to describe the structure of $BaPbO_{3-\delta}$ at room temperature, which has been confirmed to crystalize in the space group $Imma$ with $a \approx 6.030$ Å, $b \approx 8.509$ Å, and $c \approx 6.069$ Å.[5,52–54] There are four Ba, four Pb, and twelve O in the unit cell of $BaPbO_{3-\delta}$, where the crystallographically independent Ba, Pb, and O are one, one, and two, respectively. A continuous solid solution for $BaBi_{1-y}Pb_yO_{3-\delta}$ ($0.0 \leq y \leq 1.0$) is not expected because the two end members $BaBiO_{3-\delta}$ and $BaPbO_{3-\delta}$ crystalize in different space groups, $P1$ and $Imma$, respectively. After careful checking, it has been found that $BaBi_{1-y}Pb_yO_{3-\delta}$ crystallizes in the $P1$ space group when $0.0 \leq y \leq 0.88$ and in the $Imma$ space group when $0.93 \leq y \leq 1.0$ with a two-phase region between them,[5] which agrees well with the Gibbs phase rule.[55–57] Therefore, the $P1$ space group ($a \approx 6.141$ Å, $b \approx 6.186$ Å, $c \approx 6.144$ Å, $\alpha \approx 59.90°$, $\beta \approx 59.98°$, and $\gamma \approx 59.87°$) is suggested to describe the structure of $BaBi_{0.25}Pb_{0.75}O_{3-\delta}$.

As shown in Fig. 2, the Rietveld refinement of the X-ray and neutron diffraction data of $BaBi_{0.25}Pb_{0.75}O_{3-\delta}$ (the sample In1) could be performed well using the space group $P1$ with the corresponding parameters listed in Table 1. Two diffractions (004 and 220) are expected in the region from 41 to 43° of two theta or 2.12 to 2.16 Å of d value by the space groups $Im/4cm$
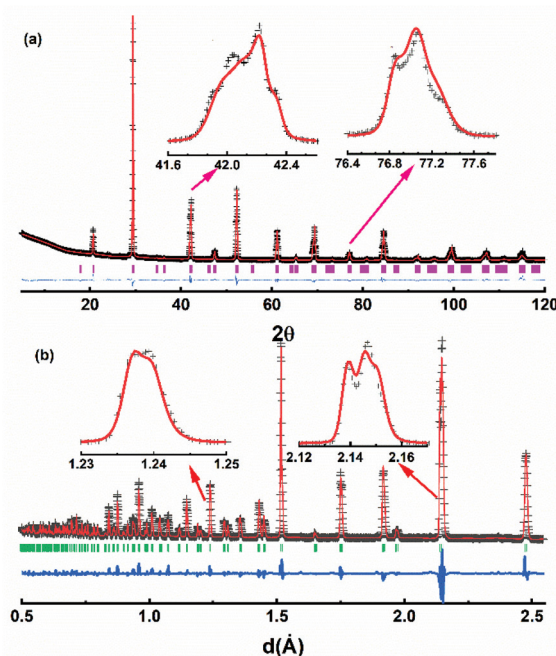

Fig. 2 Rietveld plot of the X-ray (a) and neutron (b) diffraction data for $BaBi_{0.25}Pb_{0.75}O_{3-\delta}$ using the space group $P1$. The plus symbol represents the observed value, the solid line represents the calculated value, the marks below the diffraction patterns are the calculated reflection positions, and the difference curve is shown at the bottom in the figure.

Table 1 Rietveld refinement details of the X-ray and neutron diffraction data for $BaBi_{0.25}Pb_{0.75}O_{3-\delta}$ in the space group $P1$

Lattice parameter	$a = 6.0629(2)$ Å, $b = 6.0574(3)$ Å, $c = 6.0681(3)$ Å, $\alpha = 60.24(1)°$, $\beta = 59.91(2)°$, $\gamma = 60.02(2)°$		
Atom	x, y, z	Occupancy	U_{iso}
Ba1	0.2498(1), 0.2464(2), 0.2368(1)	1.000	0.0036(2)
Ba2	0.7527(3), 0.7399(2), 0.7411(2)	1.000	0.0044(2)
Bi1/Pb1	0.0000, 0.0000, 0.0000	0.250/0.750	0.0029(4)
Bi2/Pb2	0.5023(2), 0.4912(2), 0.5004(3)	0.250/0.750	0.0047(4)
O1	0.2989(3), 0.1857(3), 0.7394(4)	0.986(6)	0.0075(5)
O2	0.7177(4), 0.7787(3), 0.2759(4)	0.985(5)	0.0074(4)
O3	0.7676(4), 0.2505(2), 0.2448(3)	0.986(4)	0.0088(5)
O4	0.2477(3), 0.6754(4), 0.8170(4)	0.986(5)	0.0075(4)
O5	0.2347(3), 0.7544(4), 0.2754(3)	0.986(4)	0.0088(5)
O6	0.7565(3), 0.2578(3), 0.7495(3)	0.985(5)	0.0075(3)
R factor[a]	$R_{wp}^x = 0.048$, $R_p^x = 0.031$; $R_{wp}^n = 0.073$, $R_p^n = 0.057$		

[a] R_{wp}^x, R_p^x and R_{wp}^n, R_p^n are the R factors of the whole patterns and the peaks for X-ray (x) and neutron (n) diffraction data, respectively.

and $Ibmm$; three diffractions (004, −220 and 220) are expected by the space groups $I2/m$ and Im; three diffractions (202, 220 and 022) are expected by the space group $P1$. In addition, one diffraction (404) is expected in the region from 76 to 78° of two theta or 1.23 to 1.25 Å of d value by the space group $Im/4cm$; two diffractions (404 and 044) are expected by the space groups $Ibmm$, $I2/m$ and Im; four diffractions (004, 040, 400 and 444) are expected by the space group $P1$. As shown in inset of
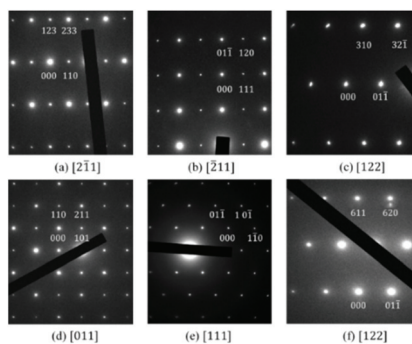
This journal is © the Partner Organisations 2020

Inorg. Chem. Front., 2020, **7**, 3561–3570 | **3563**

Fig. 3 SAED patterns of $BaBi_{0.25}Pb_{0.75}O_{3-\delta}$ (a–c) and $Ba(Bi_{0.25}Pb_{0.75})_{0.96}In_{0.04}O_{3-\delta}$ (d–f) along different directions.

Fig. 2, three diffractions are found in the region from 41 to 43° of two theta or 2.12 to 2.16 Å of d value and more than two diffractions are found in the region from 76 to 78° of two theta or 1.23 to 1.25 Å of d value. Therefore, the space group $P1$ is suitable to describe the structure of the sample $BaBi_{0.25}Pb_{0.75}O_{3-\delta}$ synthesized in our lab.

Selected area electron diffraction (SAED) are useful to confirm the space group of the studied sample.[5,58] Therefore, SAED patterns of $BaBi_{0.25}Pb_{0.75}O_{3-\delta}$ have been checked. Typical data are shown in Fig. 3. These patterns can be well indexed by the space group $P1$ with $a \approx 6.063$ Å, $b \approx 6.057$ Å, $c \approx 6.070$ Å, $\alpha \approx 60.23°$, $\beta \approx 59.87°$, and $\gamma \approx 60.04°$, which indicates it is acceptable to use the $P1$ space group to describe the structure of $BaBi_{0.25}Pb_{0.75}O_{3-\delta}$. The present lattice parameters are very close to rhombohedral with $a \approx b \approx c \approx 6.06$ Å and $\alpha \approx \beta \approx \gamma \approx 60.0°$. The unit cell looks like a rhombohedron, as shown in Fig. 4. There are two crystallographically independent sites for Ba and six sites for O in the unit cell. There are also two crystallographically independent sites randomly occupied by Bi or Pb with the ratio of 0.25 : 0.75.

In fact, one may find that the X-ray and neutron diffraction data of the sample In1 can be refined well using the space group $P\bar{1}$ with $a \approx 6.063$ Å, $b \approx 6.057$ Å, $c \approx 6.070$ Å, $\alpha \approx 60.23°$, $\beta \approx 59.87°$ and $\gamma \approx 60.04°$ (the other details are listed in Table S1 of the ESI‡). The refinement is improved just a little using the $P1$ space group than $P\bar{1}$. One can attribute this to the fact that more parameters are refined when the $P1$ space group is used. Does this mean the $P\bar{1}$ space group is a good choice? For comparison, the X-ray and neutron diffraction data of
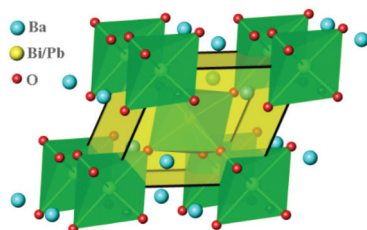
$BaBiO_{3-\delta}$ in our previous work are also checked to confirm the Rietveld refinement using the $P\bar{1}$ space group with the same lattice parameters published for the $P1$ space group[20] with Ba (0.2519(2), 0.2532(2), 0.2454(1)), Bi1 (0.0000, 0.0000, 0.0000), Bi2 (0.5000, 0.5000, 0.5000), O1 (0.2206(3), 0.3012(2), 0.7038(4)), O2 (0.7124(3), 0.2815(3), 0.2310(2)), and O3 (0.2710(4), 0.8032(3), 0.2480(3)). Two crystallographically independent sites are set for Bi. The refinement is also improved just a little using the $P1$ space group rather than $P\bar{1}$ for $BaBiO_3$ (see the ESI‡). These results may indicate that sometimes it is difficult to find the difference between $P1$ and $P\bar{1}$ using the Rietveld refinement. In this case, the idea "the activities in Raman and infrared spectroscopy are mutually exclusive in a crystal with inversion symmetry" mentioned by S. Sugai[48] seems to provide us with a possible way to solve such a question. Then, the Raman and infrared spectra of the sample In1 are obtained. As shown in Fig. 5, the partial overlaps of the Raman peaks and infrared peaks for In1 indicate that there is no inversion symmetry for In1. Therefore, it is a good choice to use the $P1$ space group to describe the structure of In1.

The SAED patterns of the samples In2 to In13 can also be indexed well with the space group $P1$ using similar lattice parameters of $BaBi_{0.25}Pb_{0.75}O_{3-\delta}$ as shown in Fig. 3 for the sample In5. In addition, the Raman peaks and infrared peaks of In5 and In9 are partially overlapped, as shown in Fig. 5. Therefore, the structure of $BaBi_{0.25}Pb_{0.75}O_{3-\delta}$ is used as the starting model to refine the X-ray diffraction data of In2 to In13. These data can be refined well with $R_{wp} < 0.062$ and $R_p < 0.039$ as shown in Fig. 6a and c for the samples In5 and In9, respectively. After these refinements, the volume of the unit cell of each sample can be obtained. The corresponding data are shown in Fig. 7. The volume of the unit cell decreases linearly with an increase of indium in the sample, which agrees well with Vegard's law.[59,60] This may be due to the fact that the average ionic radius of B site decreases with the increase of indium in the sample. For simplicity, one can just suggest that there are 0.125 Bi^{3+}, 0.125 Bi^{5+}, and 0.75 Pb^{4+} in $BaBi_{0.25}Pb_{0.75}O_{3-\delta}$ (although in the next section, it is found that Pb^{2+} ion is also present in the sample due to oxygen vacancy) with $\delta = 0$. The average ionic radius of B site is about $0.125\, r_{Bi^{3+}} + 0.125\, r_{Bi^{5+}} + 0.75\, r_{Pb^{4+}}$. For $Ba(Bi_{0.25}Pb_{0.75})_{1-x}In_xO_{3-\delta}$, one can simply assume x In^{3+} replace 0.125x Bi^{3+} + 0.125x Bi^{5+} + 0.75x Pb^{4+} and force the change from 0.5x Bi^{3+} to 0.5x Bi^{5+} when $\delta = 0$. In this case, the average ionic radius of B site is about $(0.125-0.625x)\, r_{Bi^{3+}} + (0.125 + 0.375x)r_{Bi^{5+}} + (0.75-0.75x)\, r_{Pb^{4+}} + x r_{In^{3+}}$. The difference is $(-0.625 r_{Bi^{3+}} + 0.375 r_{Bi^{5+}} -$

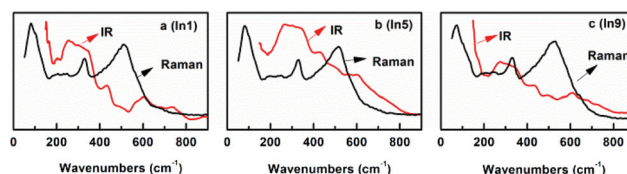**Fig. 4** Crystal structure of $BaBi_{0.25}Pb_{0.75}O_{3-\delta}$.

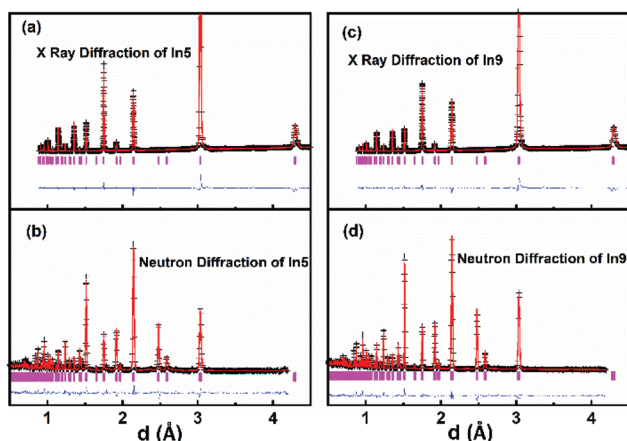**Fig. 5** Raman and infrared spectra of In1 (a), In5 (b), and In9 (c).

Fig. 6 Rietveld plot of the X-ray and neutron diffraction data of the samples In5 (a and b) and In9 (c and d) at room temperature. The plus symbol represents the observed value, the solid line represents the calculated value, the marks below the diffraction patterns are the calculated reflection positions, and the difference curve is shown at the bottom in the figure.
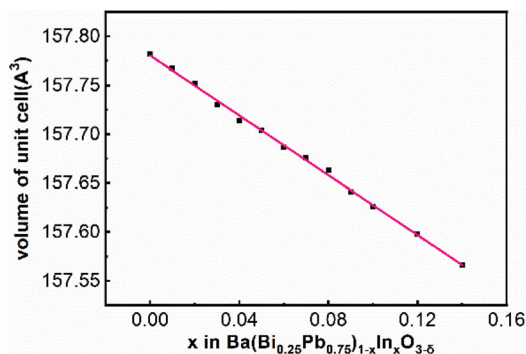

Fig. 7 Volume of the unit cell of $Ba(Bi_{0.25}Pb_{0.75})_{1-x}In_xO_{3-\delta}$ at room temperature.

$0.75r_{Pb^{4+}} + r_{In^{3+}})x$. It is known that $r_{Bi^{3+}} = 1.03$ Å (six coordinated), $r_{Bi^{5+}} = 0.76$ Å (six coordinated), $r_{Pb^{4+}} = 0.775$ Å (six coordinated) and $r_{In^{3+}} = 0.80$ Å (six coordinated). Then, the difference is about $-0.14x$. Therefore, with an increase of In^{3+} in the sample $Ba(Bi_{0.25}Pb_{0.75})_{1-x}In_xO_{3-\delta}$, the average radius of the ion at the B site decreases, which causes the decrease of the volume of the unit cell.

As well known, the Rietveld refinement of the powder X-ray diffraction data is not sensitive to oxygen (its position and occupation) when there are heavy atoms such as Ba, Bi, or Pb in the unit cell. Therefore, three samples In1, In5 and In9 are chosen to collect the neutron diffraction data to assess the occupancy of oxygen at its crystallographic site by the Rietveld refinement. This information is important due to the fact that oxygen vacancy could change the structure and properties such as that reported for $BaBi_{0.25}Pb_{0.75}O_{3-\delta}$.[29-31] The combined Rietveld refinement of powder neutron diffraction data and X-ray diffraction data are performed well for these

samples with $R_{wp} < 0.073$ and $R_p < 0.057$. Rietveld plots are shown in Fig. 6 for In5 and In9 (the one for In1 is shown in Fig. 2). The crystallographic data, and structural parameters for In5 and In9 are tabulated in Table 2. There is no obvious difference among the oxygen occupancy at the six crystallographic oxygen sites. Oxygen deficiency increases slightly from In5 to In9.

It should be mentioned that the samples with the nominal formula $Ba(Bi_{0.25}Pb_{0.75})_{1-x}In_xO_{3-\delta}$ ($0.14 < x \leq 0.25$) have also been synthesized in our lab. The upper substitution limit is around $x = 0.20$. However, for some reason, the results of the resistance measurement for the samples $Ba(Bi_{0.25}Pb_{0.75})_{1-x}In_xO_{3-\delta}$ ($0.14 < x \leq 0.25$) are not stable. These data are not suitable to be published at present.

Valence of the elements in $Ba(Bi_{0.25}Pb_{0.75})_{1-x}In_xO_{3-\delta}$

Valence of the element in a compound has an important effect on its lattice parameters, which has been mentioned in the above section and has also been discussed in a previous work.[9] In addition, the valence of the element in oxide compounds has a strong relationship to the oxygen vacancy. Therefore, XPS spectra of $Ba(Bi_{0.25}Pb_{0.75})_{1-x}In_xO_{3-\delta}$ are obtained for several selected samples. Fig. 8 shows the typical data for the samples In5 and In9. The survey shown in Fig. 8a indicates that the sample is composed of Ba, Bi, Pb, In, and O elements, while the C element is ascribed to be calibrated from the XPS instrument itself. Two symmetric peaks located at 779.53 eV and 794.83 eV in Fig. 8b correspond to Ba $3d_{5/2}$ and Ba $3d_{3/2}$ of Ba^{2+} ions in the perovskite structure.[61] No obvious change could be observed in the XPS spectra of Ba $3d_{5/2}$ or Ba $3d_{3/2}$ for In5 and In9, respectively. The XPS spectra of Bi $4f_{7/2}$ (Pb $4f_{7/2}$) and Bi $4f_{5/2}$ (Pb $4f_{5/2}$) are doublets, as shown in Fig. 8c and d. The higher binding energy peaks of Bi $4f_{7/2}$ (Pb $4f_{7/2}$) and Bi $4f_{5/2}$ (Pb $4f_{5/2}$) around 159.03 eV (139.33 eV) and 164.28 eV (143.16 eV) are characteristic peaks for $Bi^{5+}(Pb^{4+})$.[9,10,62,63] The lower binding energy peaks of Bi $4f_{7/2}$ (Pb $4f_{7/2}$) and Bi $4f_{5/2}$ (Pb $4f_{5/2}$) around 158.19 eV (137.20 eV) and 163.48 eV (142.07 eV) are characteristic peaks for $Bi^{3+}(Pb^{2+})$.[9,10] The peaks corresponding to $Bi^{5+}(Pb^{4+})$ for In9 are larger than that of In5, which may mean more $Bi^{5+}(Pb^{4+})$ in the sample In9.

The peaks at the binding energy of 443.52 eV and 451.73 eV in Fig. 8e could be assigned to $3d_{5/2}$ and $3d_{3/2}$ for In^{3+}.[63,64] The broad peak near $3d_{5/2}$ of In^{3+} can be divided into two peaks with a binding energy of about 441.6 eV and 440.1 eV corresponding to $4d_{3/2}$ for Bi^{5+} and Bi^{3+}, respectively. It is reasonable that the intensity of In^{3+} $3d_{3/2}$ for In9 is stronger than that for In5 as there are more indium atoms in the sample In9.

The spectrum of O 1s has two components O1 1s and O2 1s, as shown in Fig. 8f. O1 1s is at around 528.96 eV, which corresponds to O^{2-} ions without the oxygen vacancy in the first near neighbor.[61,63,65,66] O2 1s is at about 531.01 eV, which can be associated with O^{2-} ions with the oxygen vacancy in the first near neighbor.[61,65,66] The intensity of O2 1s of In9 is stronger than that of In5, which may mean that more oxygen vacancy exists in the sample In9 than In5.

Table 2 Rietveld refinement details of the X-ray and neutron diffraction data for In5 and In9

	In5			In9		
Space group	P1			P1		
Lattice parameter	$a = 6.0657(1)$ Å, $b = 6.0582(3)$ Å, $c = 6.0640(2)$ Å, $\alpha = 60.20(1)°$, $\beta = 59.86(3)°$, $\gamma = 60.06(2)°$			$a = 6.0646(1)$ Å, $b = 6.0600(3)$ Å, $c = 6.0603(2)$ Å, $\alpha = 60.26(2)°$, $\beta = 59.82(2)°$, $\gamma = 60.07(3)°$		
Atom	x, y, z	Occupancy	U_{iso}	x, y, z	Occupancy	U_{iso}
Ba1	0.2512(1), 0.2681(2), 0.2387(1)	1.000	0.0051(4)	0.2484(2), 0.2666(1), 0.2441(2)	1.000	0.0058(3)
Ba2	0.7522(3), 0.7628(2), 0.7434(3)	1.000	0.0082(3)	0.7452(3), 0.7710(2), 0.7414(3)	1.000	0.0058(3)
Bi/Pb/In1	0.0000, 0.0000, 0.0000	0.240/0.720/0.040	0.0076(5)	0.0000, 0.0000, 0.0000	0.230/0.690/0.080	0.0081(4)
Bi/Pb/In2	0.4988(2), 0.4978(2), 0.5032(3)	0.240/0.720/0.040	0.0070(5)	0.5009(3), 0.4971(2), 0.5019(2)	0.230/0.690/0.080	0.0074(4)
O1	0.2638(2), −0.2036(1), 0.7072(3)	0.986(6)	0.0138(6)	0.2648(1), −0.2204(1), 0.7219(3)	0.982(6)	0.0108(5)
O2	0.7652(3), 0.7290(3), 0.2391(1)	0.985(5)	0.0080(5)	0.7746(3), 0.7158(2), 0.2206(1)	0.983(6)	0.0118(6)
O3	0.7383(3), 0.2090(1), 0.2878(2)	0.988(5)	0.0075(4)	0.7570(3), 0.2095(1), 0.2787(2)	0.982(5)	0.0098(5)
O4	0.2095(1), 0.2892(2), 0.7898(3)	0.986(6)	0.0155(5)	0.2355(1), 0.2667(2), 0.7986(3)	0.982(6)	0.0161(6)
O5	0.2349(1), 0.7255(3), 0.2713(2)	0.987(6)	0.0154(4)	0.2532(1), 0.6947(3), 0.2606(2)	0.982(6)	0.0173(6)
O6	0.7260(3), 0.2359(2), 0.7762(3)	0.986(6)	0.0130(5)	0.7471(3), 0.2314(1), 0.7569(2)	0.983(5)	0.0110(5)
R factor[a]	$R_{wp}^{x} = 0.038$, $R_{p}^{x} = 0.026$; $R_{wp}^{n} = 0.057$, $R_{p}^{n} = 0.043$			$R_{wp}^{x} = 0.043$, $R_{p}^{x} = 0.029$; $R_{wp}^{h} = 0.057$, $R_{p}^{n} = 0.048$		

[a] R_{wp}^{x}, R_{p}^{x} and R_{wp}^{n}, R_{p}^{n} are the R factors of the whole patterns and the peaks for X-ray and neutron diffraction data, respectively.
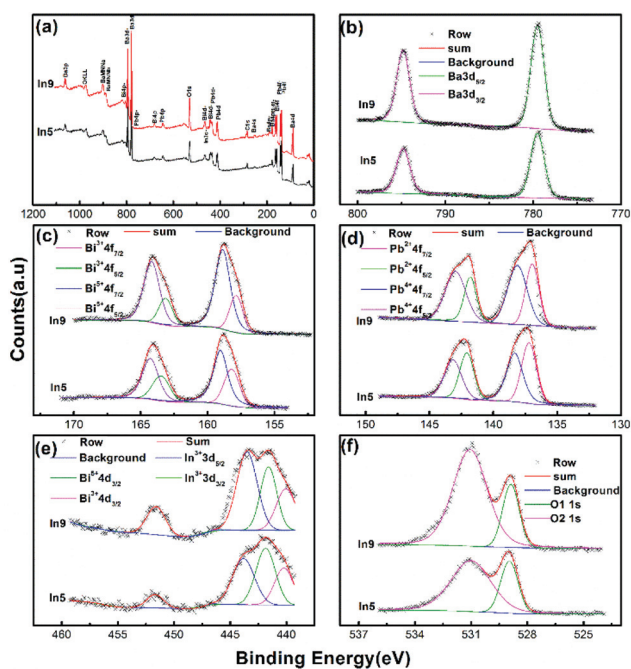

Fig. 8 Binding energies of the survey (a), Ba 3d (b), Bi 4f (c), Pb 4f (d), In 3d (e), and O 1s (f) spectra of $Ba(Bi_{0.25}Pb_{0.75})_{1-x}In_xO_{3-\delta}$ (In5 with $x = 0.04$ and In9 with $x = 0.08$).

Fig. 9 The composition-dependent oxygen vacancy δ (a) and electrons per 6S orbital (b) of $Ba(Bi_{0.25}Pb_{0.75})_{1-x}In_xO_{3-\delta}$.

Oxygen vacancy in $Ba(Bi_{0.25}Pb_{0.75})_{1-x}In_xO_{3-\delta}$

XPS data and Rietveld refinements of the neutron diffraction data of In5 and In9 indicate that there are oxygen vacancies in the samples. In order to evaluate the quantity of the oxygen vacancies in the sample, an iodometric titration is performed for several samples. As shown in Fig. 9a, the oxygen vacancies
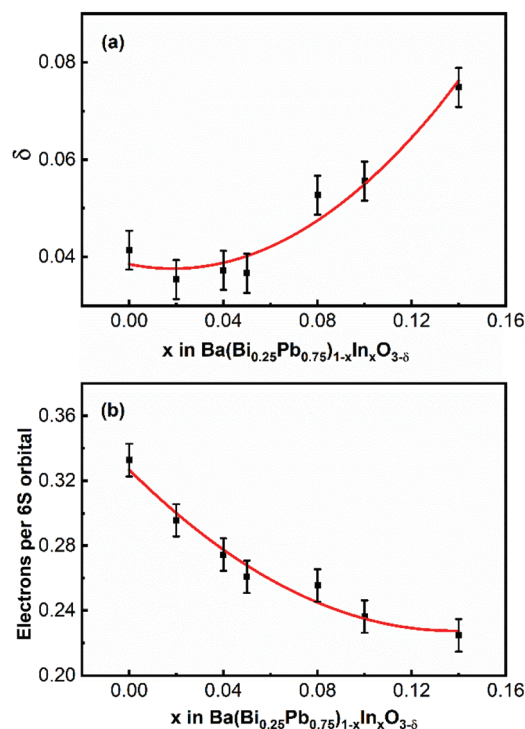
first decrease and then increase with an increase of indium in the samples. The content of oxygen vacancy of In5 is less than that of In9. This agrees well with the result obtained from the XPS spectra shown in Fig. 8f and the Rietveld refinement of the neutron diffraction data of In5 and In9. Under the consideration that the samples are neutral, one can evaluate the

3566 | *Inorg. Chem. Front.*, 2020, **7**, 3561–3570

This journal is © the Partner Organisations 2020

number of electrons per 6S orbital from the obtained value of oxygen vacancy in the samples, which decreases with an increase of indium in the samples, as shown in Fig. 9b. This means that the content of holes in the samples increases.

Superconductivity of $Ba(Bi_{0.25}Pb_{0.75})_{1-x}In_xO_{3-\delta}$

All the samples $Ba(Bi_{0.25}Pb_{0.75})_{1-x}In_xO_{3-\delta}$ $(0.00 \leq x \leq 0.14)$ are superconductors. Typical temperature-dependent resistivity is shown in Fig. 10a–c for the samples In1, In5 and In13, respectively. The electric resistivity first slightly decreases for the sample In1, or increases for the samples In5 and In13 when the temperature of the sample decreases and then abruptly decreases at a certain temperature (which is noted as T_c^{onset}), indicating the metallic or semiconducting behavior above this temperature. The electric resistivity becomes zero at a lower temperature (noted as T_c^{zero}) when the temperature is decreased further. T_c^{onset} and T_c^{zero} for $BaBi_{0.25}Pb_{0.75}O_{3-\delta}$ synthesized in our lab are 11.8 K and 10.4 K, respectively. These agree well with the previous data reported by other researchers.[1,22,67] T_c^{zero} of $Ba(Bi_{0.25}Pb_{0.75})_{1-x}In_xO_{3-\delta}$ decreases with an increase of indium in the samples, as shown in Fig. 10d. This decrease may be due to the fact that $Ba(Bi_{0.25}Pb_{0.75})_{1-x}In_xO_{3-\delta}$ departs from the optimal hole-doping state of $BaBi_{0.25}Pb_{0.75}O_{3-\delta}$ with an increase of indium in the samples. As discussed in Oxygen vacancy in $Ba(Bi_{0.25}Pb_{0.75})_{1-x}In_xO_{3-\delta}$, the increase of indium in the sample $Ba(Bi_{0.25}Pb_{0.75})_{1-x}In_xO_{3-\delta}$ will decrease electrons in the 6S orbital, which means that holes increase. $BaBi_{0.25}Pb_{0.75}O_{3-\delta}$ is reported to be an optimal hole-doped superconductor.[67] Therefore, $Ba(Bi_{0.25}Pb_{0.75})_{1-x}In_xO_{3-\delta}$ will depart from the optimal hole-doping state to let the corresponding T_c^{zero} decrease with an increase of indium.

It is interesting that T_c^{onset} of $Ba(Bi_{0.25}Pb_{0.75})_{1-x}In_xO_{3-\delta}$ decreases more slowly than T_c^{zero} as shown in the inset of Fig. 8d. This means that $\Delta T (=T_c^{onset} - T_c^{zero})$ increases with an increase of indium. Does this indicate that the homogeneity of $Ba(Bi_{0.25}Pb_{0.75})_{1-x}In_xO_{3-\delta}$ becomes worse with more different atoms at the B site when more indium is doped into the sample? The present data could not give a clear answer. Maybe the change of synthesis conditions can narrow ΔT.

Conclusions

Indium has been successfully doped into the B site of $BaBi_{0.25}Pb_{0.75}O_{3-\delta}$ to form solid solutions $Ba(Bi_{0.25}Pb_{0.75})_{1-x}In_xO_{3-\delta}$ $(0 \leq x \leq 0.14)$ by a solid state reaction at temperatures from 780 °C to 880 °C. They all crystalize in the $P1$ space group confirmed by selected area electron, X-ray, and neutron diffraction data. The resistivity of the samples was measured between 3 K and 50 K, which indicates that all the studied samples show superconductivity. T_c^{zero} of $Ba(Bi_{0.25}Pb_{0.75})_{1-x}In_xO_{3-\delta}$ decreases with an increase of indium in the samples, which is due to the fact that the content of holes departs from the optimal doping state of $BaBi_{0.25}Pb_{0.75}O_{3-\delta}$.

Conflicts of interest

There are no conflicts to declare.

Acknowledgements

Notes and references

1 A. W. Sleight, J. L. Gillson and P. E. Bierstedt, High-temperature superconductivity in $BaPb_{1-x}Bi_xO_3$ system, *Solid State Commun.*, 1975, **17**, 27–28.

2 R. J. Cava, B. Batlogg, J. J. Krajewski, R. Farrow, L. W. Rupp, A. E. White, K. Short, W. F. Peck and T. Kometani, Superconductivity near 30 K without copper - the $Ba_{0.6}k_{0.4}BiO_3$ perovskite, *Nature*, 1988, **332**, 814–816.

3 M. Braden, W. Reichardt, E. Elkaim, J. P. Lauriat, S. Shiryaev and S. N. Barilo, Structural distortion in superconducting $Ba_{1-x}K_xBiO_3$, *Phys. Rev. B: Condens. Matter Mater. Phys.*, 2000, **62**, 6708–6715.

4 M. H. Rubel, A. Miura, T. Takei, N. Kumada, M. Mozahar Ali, M. Nagao, S. Watauchi, I. Tanaka, K. Oka, M. Azuma, E. Magome, C. Moriyoshi, Y. Kuroiwa and A. K. M. Azharul Islam, Superconducting double perovskite Bismuth oxide prepared by a low-temperature hydrothermal reaction, *Angew. Chem., Int. Ed.*, 2014, **53**, 3599–3603.

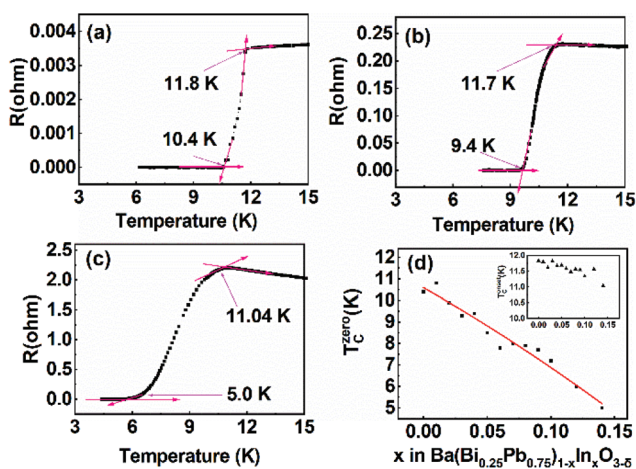**Fig. 10** Temperature-dependent resistance of In1 (a), In5 (b) and In13 (c), and composition-dependent T_c^{zero} of $Ba(Bi_{0.25}Pb_{0.75})_{1-x}In_xO_{3-\delta}$ (d).

This journal is © the Partner Organisations 2020

Inorg. Chem. Front., 2020, **7**, 3561–3570 | **3567**

5 H. Zhang, X. H. Lin, Y. T. Zheng, S. E. Li, G. B. Li, F. H. Liao and J. H. Lin, Synthesis, structure, and properties of the superconductor $Ba_{1-x}K_zBi_{1-y}Pb_yO_3$, *J. Supercond. Novel Magn.*, 2015, **28**, 459–467.

6 M. A. Farid, F. Y. Zhang, M. Zhang, H. X. Zhang, A. Firdous, G. B. Li, F. H. Liao and J. H. Lin, Superconductivity for potassium doped $BaPb_{0.80}Bi_{0.20}O_{3\text{-delta}}$ and $BaPb_{0.60}Bi_{0.40}O_{3\text{-delta}}$ with zero electrical resistivity at ∼11 K, *J. Alloys Compd.*, 2020, **815**, 152460.

7 L. F. Mattheiss, E. M. Gyorgy and D. W. Johnson, Superconductivity above 20 K in the Ba-K-Bi-O system, *Phys. Rev. B: Condens. Matter Mater. Phys.*, 1988, **37**, 3745–3746.

8 M. Zhang, M. A. Farid, H. Zhang, J. L. Sun, G. B. Li, F. H. Liao and J. H. Lin, Superconductivity of Perovskite $Ba_{1-x}Y_x(Bi_{0.2}Pb_{0.8})O_{3-\text{delta}}$, *J. Supercond. Novel Magn.*, 2017, **30**, 1705–1712.

9 M. Zhang, M. A. Farid, Y. Wang, J. L. Xie, J. L. Geng, H. Zhang, J. L. Sun, G. B. Li, F. H. Liao and J. H. Lin, Superconductivity in Perovskite $Ba_{1-x}Ln_x(Bi_{0.20}Pb_{0.80})O_{3-\delta}$ (Ln=La, Ce, Pr, Nd, Sm, Eu, Gd, Tb, Dy, Ho, Er, Tm, Yb, Lu), *Inorg. Chem.*, 2018, **57**, 1269–1276.

10 A. Firdous, X. G. Wang, M. A. Farid, M. Zhang, Y. Wang, J. L. Geng, J. L. Sun, G. B. Li, F. H. Liao and J. H. Lin, Superconductivity in Perovskite $Ba_{0.85-x}La_xPr_{0.15}(Bi_{0.20}Pb_{0.80})O_{3-\delta}$, *J. Supercond. Novel Magn.*, 2019, **32**, 167–173.

11 M. H. K. Rubel, T. Takei, N. Kumada, M. M. Ali, A. Miura, K. Tadanaga, K. Oka, M. Azuma, M. Yashima, K. Fujii, E. Magome, C. Moriyoshi, Y. Kuroiwa, J. R. Hester and M. Aydeev, Hydrothermal Synthesis, Crystal Structure, and Superconductivity of a Double-Perovskite Bi Oxide, *Chem. Mater.*, 2016, **28**, 459–465.

12 Z. Iqbal, G. H. Kwei, B. L. Ramakrishna and E. W. Ong, Structure and Bulk Superconductivity of $BaPb_{0.5}Bi_{0.25}Tl_{0.25}O_{3-\text{Delta}}$, *Phys. C*, 1990, **167**, 369–374.

13 N. R. Khasanova, F. Izumi, T. Kamiyama, K. Yoshida, A. Yamamoto and S. Tajima, Crystal structure of the $(K_{0.87}Bi_{0.13})BiO_3$ superconductor, *J. Solid State Chem.*, 1999, **144**, 205–208.

14 S. M. Kazakov, C. Chaillout, P. Bordet, J. J. Capponi, M. Nunez-Regueiro, A. Rysak, J. L. Tholence, P. G. Radaelli, S. N. Putilin and E. V. Antipov, Discovery of a second family of bismuth-oxide-based superconductors, *Nature*, 1997, **390**, 148–150.

15 M. H. K. Rubel, T. Takei, N. Kumada, M. M. Ali, A. Miura, K. Tadanaga, K. Oka, M. Azuma, E. Magomae, C. Moriyoshi and Y. Kuroiwa, Hydrothermal Synthesis of a New Bi-based $(Ba_{0.82}K_{0.18})(Bi_{0.53}Pb_{0.47})O_3$ Superconductor, *J. Alloys Compd.*, 2015, **634**, 208–214.

16 M. H. K. Rubel, T. Takei, N. Kumada, M. M. Ali, A. Miura, K. Tadanaga, K. Oka, M. Azuma, E. Magome, C. Moriyoshi and Y. Kuroiwa, Hydrothermal Synthesis, Structure, and Superconductivity of Simple Cubic Perovskite $(Ba_{0.62}K_{0.38})(Bi_{0.92}Mg_{0.08})O_3$ with T_c similar to 30 K, *Inorg. Chem.*, 2017, **56**, 3174–3181.

17 R. J. Cava, B. Batlogg, G. P. Espinosa, A. P. Ramirez, J. J. Krajewski, W. Peck, L. W. Rupp and A. S. Cooper, Superconductivity at 3.5 K in $BaPb_{0.75}Sb_{0.25}O_3$ - Why Is T_c So Low, *Nature*, 1989, **339**, 291–293.

18 N. R. Khasanova, K. Yoshida, A. Yamamoto and S. Tajima, Extended Range of Superconducting Bismuthates $K_{1-x}A_xBiO_3$ (A=La, Bi, and Ca), *Phys. C*, 2001, **356**, 12–22.

19 M. A. Farid, H. Zhang, X. H. Lin, A. M. Yang, S. H. Yang, G. B. Li, F. H. Liao and J. H. Lin, Structural and magnetic properties of tetragonal perovskite $BaFe_{1-x}Bi_xO_{3-\delta}$, *RSC Adv.*, 2015, **5**, 12866–12871.

20 H. Wang, C. H. Wang, G. B. Li, T. N. Jin, F. H. Liao and J. H. Lin, Synthesis, structure, and characterization of the series $BaBi_{1-x}Ta_xO_3$ (0<=x<=0.5), *Inorg. Chem.*, 2010, **49**, 5262–5270.

21 M. A. Farid, H. Zhang, A. M. Yang, G. F. Tian, M. M. Wu, G. B. Li, F. H. Liao and J. H. Lin, Facile Synthesis, Structure Elucidation, and Magnetic Properties of Perovskite $BaTb_{1-x}Bi_xO_3$, *Eur. J. Inorg. Chem.*, 2017, 1427–1434.

22 A. W. Sleight, Bismuthates: $BaBiO_3$ and related superconducting phases, *Phys. C*, 2015, **514**, 152–165.

23 H. M. Rietveld, A profile refinement method for nuclear and magnetic structures, *J. Appl. Crystallogr.*, 1969, **2**, 65–71.

24 A. C. Larson and R. B. von Dreele, *Report LAUR 86–748. Los Alamos National Laboratory*, Los Alamos, NM, 1985.

25 D. E. Cox and A. W. Sleight, Structural Studies of the $BaPb_{1-x}Bi_xO_3$ system, *Proceedings of the Conference on Neutron Scattering, Gatlinburg, Tennessee*, ed. R. M. Moon, National Technical Information Service, Springfield, VA, 1976, pp. 45–54.

26 A. W. Sleight and D. E. Cox, Symmetry of Superconducting Compositions in the $BaPb_{1-x}Bi_xO_3$ System, *Solid State Commun.*, 1986, **58**, 347–350.

27 J. Bredthauer, N. Wagner and M. Jansen, Crystal-Growth and Structure Determination of $BaPb_{(1-x)}Bi_xO_3$ (x=0.15), *Z. Anorg. Allg. Chem.*, 1991, **593**, 193–199.

28 Y. Khan, K. Nahm, M. Rosenberg and H. Willner, Superconductivity and Semiconductor - Metal Phase-Transition in System $BaPb_{1-x}Bi_xO_3$, *Phys. Status Solidi A*, 1977, **39**, 79–86.

29 M. Oda, Y. Hidaka, A. Katsui and T. Murakami, Structural Phase-Transition in Superconducting $BaPb_{0.75}Bi_{0.25}O_3$, *Solid State Commun.*, 1985, **55**, 423–426.

30 M. Oda, Y. Hadika, A. Katsui and T. Murakami, The Crystallographic Symmetries of Single $BaPb_{1-x}Bi_xO_3$ Crystals Grown from $BaCO_3$-PbO_2-Bi_2O_3 Solutions, *Solid State Commun.*, 1986, **60**, 897–900.

31 H. Asano, M. Oda, Y. Endoh, Y. Hidaka, F. Izumi, T. Ishigaki, K. Karahashi, T. Murakami and N. Watanabe, Neutron Powder Diffraction from Polymorphs of $BaPb_{0.75}Bi_{0.25}O_3$, *Jpn. J. Appl. Phys.*, 1988, **27**, 1638–1640.

32 T. Hashimoto and H. Kawazoe, Effect of Oxygen-Deficiency on the Structure and Conduction Behavior of $BaPb_{0.75}Bi_{0.25}O_{3-\delta}$, *Solid State Commun.*, 1993, **87**, 251–254.

33 T. Hashimoto, R. Hirasawa, T. Yoshida, Y. Yonemura, H. Tanaka, J. Mizusaki and H. Tagawa, Analysis of Role of

3568 | *Inorg. Chem. Front.*, 2020, **7**, 3561–3570

This journal is © the Partner Organisations 2020

Oxygen Deficiency in Crystal-Structure and Conduction Mechanism of $BaBi_{0.25}Pb_{0.75}O_{3-\delta}$, *J. Phys. Chem. Solids*, 1995, **56**, 777–785.

34 T. Hashimoto, R. Hirasawa, J. Komiya, H. Hirai, H. Tanaka, H. Tagawa and J. Mizusaki, Oxygen Deficiency, Crystal System and Conduction Behavior of $BaBi_{0.25}Pb_{0.75}O_{3-\delta}$, *AIChE J.*, 1997, **43**, 2865–2869.

35 J. Ihringer, J. K. Maichle, W. Prandl, A. W. Hewat and Th. Wroblewski, Crystal-Structure of the Ceramic Superconductor $BaPb_{0.75}Bi_{0.25}O_3$, *Z. Phys. B: Condens. Matter*, 1991, **82**, 171–176.

36 T. Hashimoto, K. Tsuda, J. Shiono, J. Mizusaki and M. Tanaka, Determination of space group of $BaPb_{0.75}Bi_{0.25}O_3$ by convergent-beam electron diffraction, *Phys. C*, 2002, **382**, 422–430.

37 E. Climent-Pascual, N. Ni, S. Jia, Q. Huang and R. J. Cava, Polymorphism in $BaPb_{1-x}Bi_xO_3$ at the superconducting composition, *Phys. Rev. B: Condens. Matter Mater. Phys.*, 2011, **83**, 174512.

38 Y. N. Venevtsev, Ferroelectric Family of Barium Titanate, *Mater. Res. Bull.*, 1971, **6**, 1085–1096.

39 E. T. Shuvaeva and E. G. Fesenko, Synthesis and Structural Studies of Some Perovskites which Contain Bismuth, *Sov. Phys. Crystallogr.*, 1970, **14**, 926–927.

40 T. Nakamura, S. Kose and T. Sata, Paramagnetism and Semiconductivity in a Triclinic Perovskite $BaBiO_3$, *J. Phys. Soc. Jpn.*, 1971, **31**, 1284.

41 D. E. Cox and A. W. Sleight, Crystal-Structure of $Ba_2Bi^{3+}Bi^{5+}O_6$, *Solid State Commun.*, 1976, **19**, 969–973.

42 G. Thornton and A. J. Jacobson, Neutron-Diffraction Determination Of Structures of $Ba_2Sb^VBiII^IO_6$ and $Ba_2Bi^VBiII^IO_6$, *Acta Crystallogr., Sect. B: Struct. Sci.*, 1978, **34**, 351–354.

43 D. E. Cox and A. W. Sleight, Mixed-Valent $Ba_2Bi^{3+}Bi^{5+}O_6$ - Structure and Properties vs Temperature, *Acta Crystallogr., Sect. B: Struct. Sci.*, 1979, **35**, 1–10.

44 S. Y. Pei, J. D. Jorgensen, B. Dabrowski, D. G. Hinks, D. R. Richards, A. W. Mitchell, J. M. Newsam, S. K. Sinha, D. Vaknin and A. J. Jacobson, Structural Phase-Diagram of the $Ba_{1-x}K_xBiO_3$ System, *Phys. Rev. B: Condens. Matter. Phys.*, 1990, **41**, 4126–4141.

45 Y. Koyama and M. Ishimaru, Structural Transitions in the Superconducting Oxides Ba-Pb-Bi-O, *Phys. Rev. B: Condens. Matter Mater. Phys.*, 1992, **45**, 9966–9975.

46 T. Hashimoto, R. Hirasawa, T. Kobayashi, H. Hirai, H. Tagawa, J. Mizusaki, H. Toraya, M. Tanaka and K. Ohsumi, Characterization of Crystal System of $BaPb_{1-x}Bi_xO_3$ with X-ray Diffraction for Synchrotron Radiation, *Solid State Commun.*, 1997, **102**, 561–564.

47 Q. D. Zhou and B. J. Kennedy, High Temperature Structure of $BaBiO_3$ - a Synchrotron X-ray Powder Diffraction Study, *Solid State Commun.*, 2004, **132**, 389–392.

48 S. Sugai, Dimerization Model for the Metal-Semiconductor Transition in $BaPb_{1-x}Bi_xO_3$, *Phys. Rev. B: Condens. Matter Mater. Phys.*, 1987, **35**, 3621–3624.

49 T. Hashimoto, K. Tsuda, J. Shiono, J. Mizusaki and M. Tanaka, Determination of the Crystal System and Space Group of $BaBiO_3$ by Convergent-beam Electron Diffraction and X-ray Diffraction Using Synchrotron Radiation, *Phys. Rev. B: Condens. Matter Mater. Phys.*, 2001, **64**, 224114.

50 H. Wang, C. X. Yang, J. Lu, M. M. Wu, J. Su, K. Li, J. R. Zhang, G. B. Li, T. N. Jin, T. Kamiyama, F. H. Liao, J. H. Lin and Y. C. Wu, On the Structure of α-BiFeO₃, *Inorg. Chem.*, 2013, **52**, 2388–2392.

51 M. A. Farid, H. Zhang, A. M. Yang, G. F. Tian, M. M. Wu, G. B. Li, F. H. Liao and J. H. Lin, Response to "Does $BaTbO_3$ Adopt the $P1$ Symmetry?", *Eur. J. Inorg. Chem.*, 2018, 5267–5269.

52 S. M. Moussa, B. J. Kennedy and T. Vogt, Structural Variants in ABO_3 Type Perovskite Oxides: on the Structure of $BaPbO_3$, *Solid State Commun.*, 2001, **119**, 549–552.

53 J. R. Hester, C. J. Howard, B. J. Kennedy and R. Macquart, High-Temperature Structural Studies of $SrPbO_3$ and $BaPbO_3$, *Aust. J. Chem.*, 2002, **55**, 543–545.

54 W. T. Fu, D. Visser and D. J. W. IJdo, High-resolution Neutron Powder Diffraction Study on the Structure of $BaPbO_3$, *Solid State Commun.*, 2005, **134**, 647–652.

55 V. J. Lee, Generalization of Gibbs Phase Rule for Heterogeneous Chemical Equilibrium, *J. Chem. Educ.*, 1967, **44**, 164–166.

56 J. Coull and E. B. Stuart, *Equilibrium Thermodynamics*, John Wiley & Sons, New York, 1964, pp. 226–270.

57 J. W. Gibbs, *The Collected Works of J. Willard Gibbs*, Longmans, Green, & Co., New York, 1928, vol. I, pp. 56–100.

58 G. B. Li, L. P. You, W. T. Wei, Y. Lu, J. Ju, A. Wannberg, H. Rundlof, X. D. Zou, T. Yang, S. J. Tian, F. H. Liao, N. Toyota and J. H. Lin, $La_4Cu_{3-x}Zn_xMoO_{12}$: Zinc-doped cuprates with Kagome lattices, *J. Am. Chem. Soc.*, 2005, **127**, 14094–14099.

59 L. Vegard, The constitution of the mixed crystals and the filling of space of the atoms, *Eur. Phys. J. A*, 1921, **5**, 17–26.

60 L. Vegard, X-rays in the service of research on matter, *Z. Kristallogr. – Cryst. Mater.*, 1928, **67**, 239–259.

61 I. C. Kaya, V. Kalem and H. Akyildiz, Hydrothermal Synthesis of Pseudocubic $BaTiO_3$ Nanoparticles using TiO_2 Nanofibers: Study on Photocatalytic and Dielectric Properties, *Int. J. Appl. Ceram. Technol.*, 2019, **16**, 1557–1569.

62 X. Ma, A. Firdous, L. Zhang, S. J. Wu, J. X. Zhang, L. J. Liu, Y. Wang, J. L. Geng, J. L. Sun, G. B. Li, F. H. Liao and J. H. Lin, Superconductivity in Perovskite $Ba_{1-x}K_xBi_{0.30}Pb_{0.70}O_{3-\delta}$, *ChemistrySelect*, 2019, **4**, 3135–3139.

63 M. A. Hamza, A. N. El-Shazly and N. K. Allam, Facile Template-Free One-Pot Room-Temperature Synthesis of Novel m-Bi(OH)CrO₄ Microspheres, *Mater. Lett.*, 2020, **262**, 127188.

64 T. R. Sobahi, M. S. Amin and R. M. Mohamed, Enlargement of Photocatalytic Efficiency of $BaSnO_3$ by Indium Doping for Thiophene Degradation, *Appl. Nanosci.*, 2018, **8**, 557–565.

This journal is © the Partner Organisations 2020

Inorg. Chem. Front., 2020, **7**, 3561–3570 | **3569**

65 Z. M. Yang, D. Z. Zhang and H. N. Chen, MOF-derived Indium Oxide Hollow Microtubes/MoS_2 Nanoparticles for NO_2 Gas, *Sens. Actuators, B*, 2019, **300**, 127037.

66 J. Hu, Y. Liang, Y. Sun, Z. Zhao, M. Zhang, P. Li, W. Zhang, Y. Chen and S. Zhuiykov, Highly Sensitive NO_2 Detection on ppb Level by Devices Based on Pd-loaded In_2O_3 Hierarchical Microstructures, *Sens. Actuators, B*, 2017, **252**, 116–126.

67 S. Uchida, K. Kitazawa and S. Tanaka, Superconductivity and Metal-semiconductor Transition in $BaPb_{1-x}Bi_xO_3$, *Phase Transitions*, 1987, **8**, 95–128.